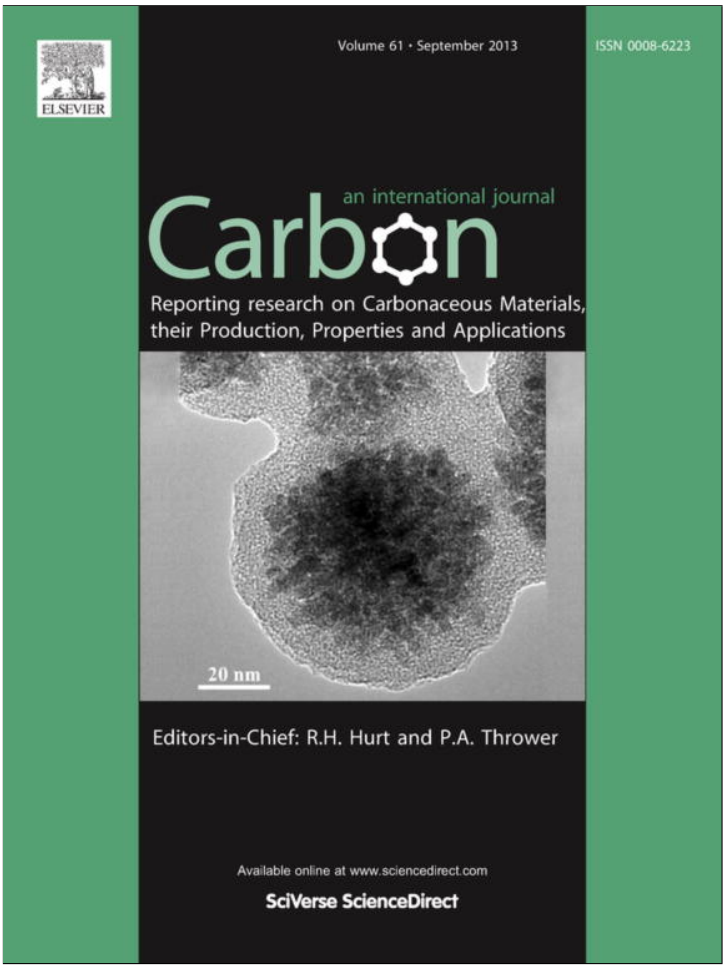

CARBON 61 (2013) 294–298

Available at www.sciencedirect.com

SciVerse ScienceDirect

journal homepage: www.elsevier.com/locate/carbon

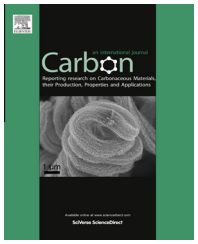

Over-barrier side-band electron emission from graphene with a time-oscillating potential

Shi-Jun Liang [a], *S. Sun* [b], *L.K. Ang* [a,b,*]

[a] *Engineering Product Development, Singapore University of Technology and Design, Singapore 138682, Singapore*
[b] *School of Electrical and Electronic Engineering, Nanyang Technological University, Singapore 639798, Singapore*

ARTICLE INFO

Article history:
Received 28 January 2013
Accepted 4 May 2013
Available online 20 May 2013

ABSTRACT

We propose a model which describes side-band electron emission from vertically aligned monolayer graphene with an internal time-oscillating barrier and a static edge barrier. Our results show that electron emission is governed by the over-barrier emission process, which is dominated by the time-oscillating barrier. The emitted current line density J [nA/nm] is only dependent on the amplitude V_1 and on the frequency ω of the time-oscillating barrier, and is characterized by $0 < \gamma = V_1/\hbar\omega < 1$. From the model, it is found that J is maximized at about $\omega = 10^{14}$ rad/s to 10^{15} rad/s, and that J increases with γ.

1. Introduction

Electron emission from nanostructures has shown great potential for various applications such as flat-panel displays [1,2], vacuum electronics [3] and compact electron sources [4–6]. The main motivation in seeking nanostructure-based electron sources is to develop an efficient electron emitter with attractive properties, such as low turn-on voltage, high current density, stable current, and long life time.

Since a monolayer graphene sheet was experimentally realized in 2004 [7], a variety of related properties have been explored including atomic thickness [8] corresponding to high aspect ratio, high electrical conductivity [9,10], and excellent mechanical strength [11,12], all of which will make graphene an ideal electron source emitter. There have been many recent experimental findings [13–19] about electron field emission from graphene and graphene composites. In their reports, they have treated the graphene as a bulk material and employed the traditional electron field emission theory known as the Fowler–Nordheim (FN) law [20] to interpret their results while introducing an arbitrarily large field enhancement factor β to account for the higher emitted current. In our recent model [21,22], we have speculated that the emission process from a monolayer vertically aligned graphene sheet exposed to a DC field can be modeled by Klein tunneling, which may increase the amount of emitted current at low applied fields.

In this paper, we propose a new mechanism for side-band electron emission from a monolayer graphene edge into vacuum induced by a time-oscillating potential. In our model, the monolayer graphene sheet with height H (50–80 nm) is vertically aligned inside a gap of spacing D (1–10 μm ≫ H). A DC voltage of V_G is applied to the gap as schematically shown in Fig. 1(a). On the planar surface of the graphene sheet (region I), we consider an internal barrier of $V = V_0 + V_1 \cos\omega t$, which is oscillating sinusoidally around V_0 with an amplitude V_1 and frequency ω. Here we have assumed that V_0, V_1 and V_G are three independent parameters. The transport of electrons from graphene into the vacuum can be divided into three parts. First, electrons tunnel through the internal potential barrier $V = V_0 + V_1 \cos\omega t$ in region I. After region I, electrons are assumed to travel ballistically (without any collisions) to reach region II. In region II, electrons are emitted through a static barrier [see Fig. 1(b)] given by $U(x) = W - \beta V_G x/D - e^2/(4\pi\varepsilon_0 x)$, where W is the work function of graphene, β is the

* *Corresponding author at:* Engineering Product Development, Singapore University of Technology and Design, Singapore 138682, Singapore.
E-mail address: ricky_ang@sutd.edu.sg (L.K. Ang).
0008-6223/$ - see front matter
http://dx.doi.org/10.1016/j.carbon.2013.05.007

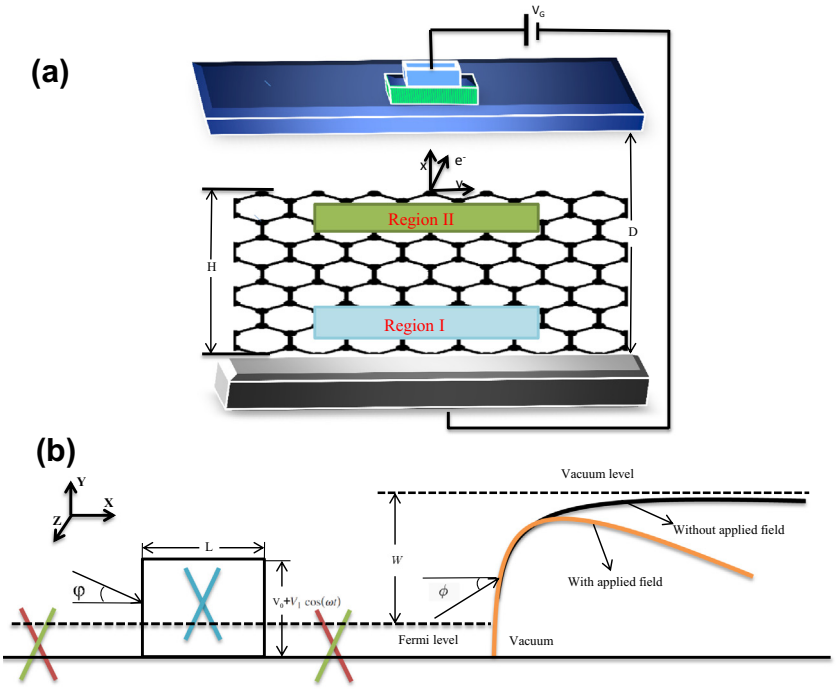

Fig. 1 – (a) Electron emission model of vertically aligned single-layer graphene sheet, where V_G is the applied voltage bias between the anode and the cathode, D (1–10 μm) is the gap spacing, H (50–80 nm) is the height of the graphene sheet. (b) Electron tunneling process in region I of a time-oscillating barrier $V = V_0 + V_1\cos(\omega t)$ with a length L and in region II of a surface barrier $U(x) = W - eFx - \frac{e^2}{4\pi\varepsilon_0 x}$, where $F = \beta V_G/D$ and W is the work function.

enhancement factor, and the last term is the classical image potential. Here, it should be mentioned that the classical image charge potential fits well with first principle simulation results, even for nanostructures like single-walled carbon nanotubes [23] and graphene [24], which show good agreement with available experimental data. Note that the image charge term can be further improved by using Thomas–Fermi approximation [25], microscopy theory [26] or first principle calculations [34]. We will compare our results in Fig. 4 with Ref. [34].

For the model to be valid, the following conditions have been assumed. The mean-free path of electrons in graphene is assumed to be much larger than the distance traveled from region I to region II, so that the transport between regions I and II can be considered collision-less. This condition is valid as long as the distance traveled is smaller than a few microns since the mean-free path can be in the range of 0.4–10 μm at room temperature [27,28].

2. Theory

We assume that the dimension along the y-axis is infinitely long, so that the boundary condition on the graphene edge can be neglected. In doing so, the emitted electron current density is expressed as the line density J [nA/nm]:

$$J = \frac{e}{2\pi^2\hbar^2 v_f}\int_0^{E_0}\int_{-\pi/2}^{\pi/2} T(E,\varphi,\phi) f(E) E\cos\phi \cdot dE \cdot d\phi, \quad (1)$$

where e is the electron charge, $\hbar$ is the reduced Planck constant, v_f (10^6 m/s) is the Fermi velocity inside graphene, and $f(E)$ is the Fermi–Dirac distribution. Here, T refers to the emission probability, which is the product of T_1 and T_2, accounting for the tunneling through the internal barrier V and the static barrier U, respectively. The other parameters φ and ϕ are, respectively, the incident angle of electrons on the time-varying barrier V and the static barrier U as shown in Fig. 1(b). Note that Eq. (1) is valid in the low energy regime where the graphene band structure remains linear (near the Dirac point). In our numerical calculation, the upper limit of the integration E_0 is 5 times higher than the Fermi energy level to avoid numerical errors. The model has not considered the coherent effects predicted by a recent microscopic theory for electron emission from graphene [26].

In region I, electrons are required to tunnel through the time-oscillating barrier of $V = V_0 + V_1\cos\omega t$ with a probability T_1. Using a recent model [29], T_1 for the first side-band is approximately given by

$$T_1 = \frac{\cos^2\phi_0}{(1-\cos^2(k_2 L)\sin^2\phi_0)}\frac{\cos^2\phi_1}{(1-\cos^2(k_2' L)\sin^2\phi_1)} \times \left(\frac{2J_1(\gamma)}{J_0(\gamma)}\right)^2 \frac{\sin^2((k_2'-k_2)L/2)}{\cos^2\phi_1} \times \left(\sin\phi_0\sin\phi_1\cos^2\left(\frac{k_2'+k_2 L}{2}\right)+\cos^2\left(\frac{\phi_0+\phi_1}{2}\right)\right), \quad (2)$$

where L is the width of the potential barrier, $\phi_0 = \tan^{-1}(k_y/k_1)$, $\phi_1 = \tan^{-1}(k_y/k_1')$, $k_1 = \sqrt{(E_1/\hbar v_f)^2 - k_y^2}$, $k_1' = \sqrt{((E_1+\hbar\omega)/\hbar v_f)^2 - k_y^2}$, $k_2 = \sqrt{((E_1-V_0)/\hbar v_f)^2 - k_y^2}$, $k_2' = \sqrt{((E_1-V_0+\hbar\omega)/\hbar v_f)^2 - k_y^2}$, k_y is the y-component of the electron wave vector, and $\gamma = V_1/\hbar\omega$. Note that Eq. (2) is only valid

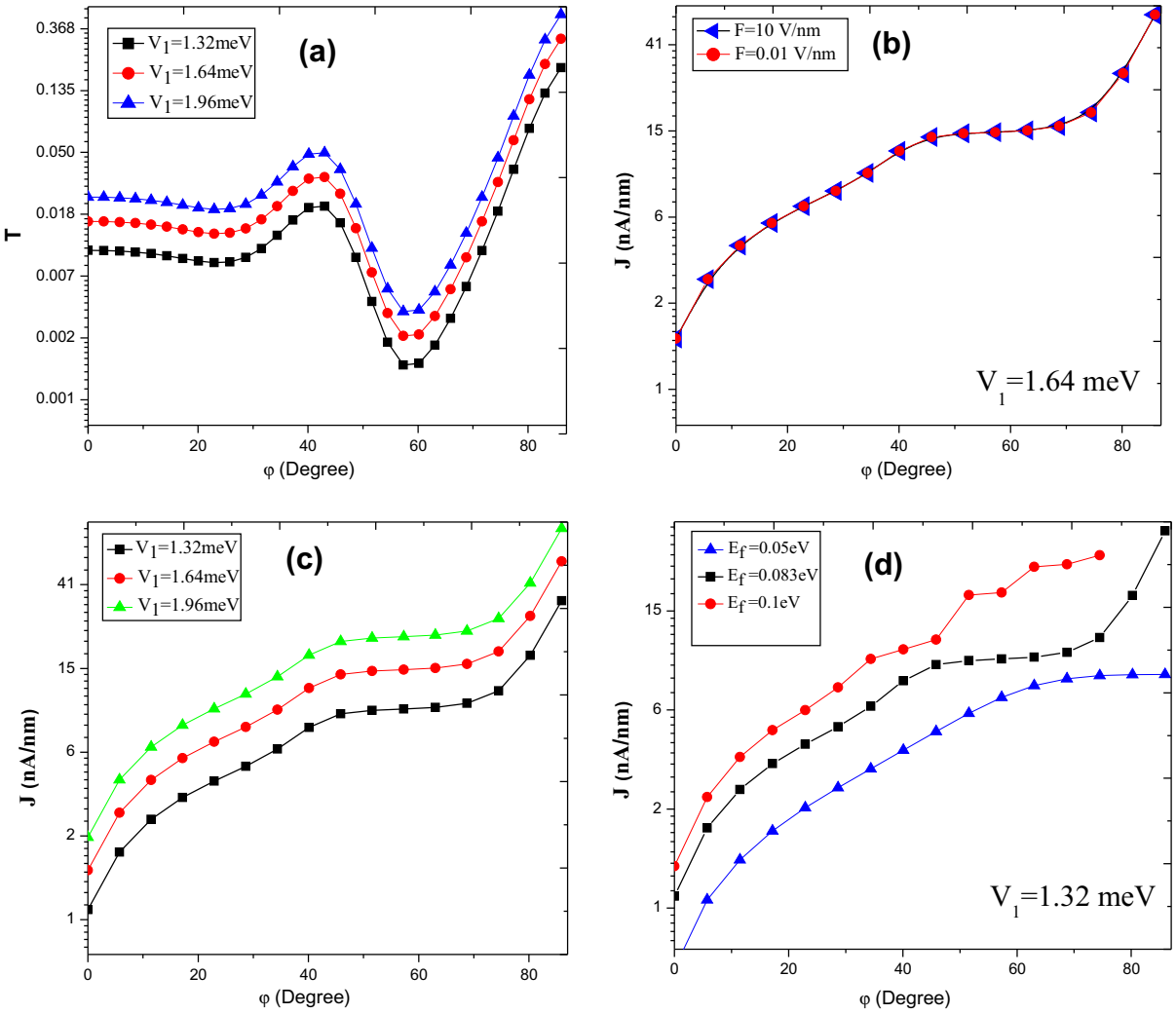

Fig. 2 – (a) The electron emission probability *T* as a function of incidence angle φ at various oscillating amplitude V_1 [meV] = 1.32, 1.64, and 1.96. The emission current line density *J* [nA/nm] as a function of incident angle φ at different (b) *F*; (c) V_1 and (d) E_f.

in the range of $0 < \gamma < 1$. For the case of $\gamma > 1$, the Dirac equation needs to be solved numerically [30].

In region II near the edge, electrons will tunnel through the static barrier $U(x) = W - \beta V_G x/D - e^2/(4\pi\varepsilon_0 x)$ with a probability T_2. Since U is a static barrier, T_2 can be calculated by employing a relativistic WKB approach [31], given by

$$T_2(E_2, \phi) = \exp^{\int_x^{x'} \frac{2}{\hbar v_f}\sqrt{sgn[(E_2 \sin\phi)^2 - (U(x)-E_2)^2]}dx}, \quad (3)$$

where *sgn* is the sign function. The sgn function appears when calculating the classical forbidden region and the classical allowed region. Here E_2 represents the electron energy along the *x*-direction after passing the internal time-oscillating potential barrier, ϕ refers to the incident angle on the static barrier *U*, *x* and *x*′ are turning points determined by $U(x) - E_2 = 0$. Note that the relativistic WKB method is found to be in good agreement with the conventional transfer matrix method [22].

The total emission probability of electrons is given by $T = T_1 \times T_2$ and the corresponding emitted current line density *J* [nA/nm] can be calculated using Eq. (1) as a function of incidence angle φ for a given set of V_0, V_1, ω, E_f and $F = \beta V_G/D$. The default values of the parameters [32,30] at room temperature (300 K) are $W = 4.66$ eV, $V_0 = 0.2$ eV, $L = 100$ nm, V_1 [meV] = 1.32, $E_f = 0.083$ eV, $F = 10$ V/nm, and $\omega = 5 \times 10^{12}$ rad/s, unless specified in the paper.

3. Results and discussion

In Fig. 2(a), we plot the total transmission probability *T* of the side band electrons at different V_1 [meV] = 1.32, 1.64 and 1.96. The figure clearly shows local maximum and minimum transmission, respectively, at around $\varphi = 40^\circ$ and $\varphi = 60^\circ$, which is due to the peculiar property of chiral tunneling of a time-oscillating potential given by T_1 [29] as shown in Eq. (2). Note that the transmission of the side-band electrons is distinctively different from that of the central band, which has a perfect transmission ($T = 1$) observed at normal incidence ($\varphi = 0^\circ$) [32]. The results also indicate that the overall

emission probability of the side band electrons is enhanced on increasing V_1 from 1.32 to 1.96 meV (see more in Fig. 2 for frequency dependence).

The emission current line density J [nA/nm] at different F, V_1 and E_f is plotted in Fig. 2(b), (c) and (d). In Fig. 2(b), we see that J is almost the same in the case of low DC field ($F = 0.01$ V/nm) and high DC field ($F = 10$ V/nm), which indicates that electron emission from the edge is dominated by over-barrier emission. The effect of the applied DC field is negligible and the static potential at the edge plays a very minor role. This finding also implies that we can control electron emission by simply tuning the relevant parameters (V_0, V_1, ω and L) to modify the internal potential barrier $V = V_0 + V_1 \cos \omega t$. On increasing V_1 from 1.32 to 1.96 meV as shown in Fig. 2(c), the electrons tunneling through the first time-oscillating barrier can reach higher energies to produce more over-barrier electrons, which leads to higher J. In general, we found that only the electrons near the Fermi energy level participate in the emission process, so J will be reduced if we decrease the Fermi energy level from 0.1 to 0.05 eV as shown in Fig. 2(d).

In Fig. 3, we study the effects of the modulation frequency ω over the range of 5×10^{12} rad/s to 5×10^{16} rad/s with $\gamma = V_1/\hbar\omega = 0.2$, 0.4 and 0.6. At a fixed γ, we find that the emitted current J is very sensitive to frequency ω. For example, at $\gamma = 0.5$ (as shown in Fig. 3(a)), J increases with ω and peaks at around $\omega = 5 \times 10^{14}$ rad/s. For $\omega < 5 \times 10^{11}$ rad/s, J is very small (<1 nA/nm). At a fixed frequency ω, J can also be increased by increasing the modulation voltage V_1 or γ ($= V_1/\hbar\omega$). In Fig. 3(b), we show the increment of J from $\gamma = 0.2$ to 0.6 at $\omega = 5 \times 10^{15}$ rad/s (dashed lines) and 5×10^{12} rad/s (solid lines).

In Fig. 4, with $F = 0$ V/nm, we compare the J obtained with different forms of the image charge potential: classical image charge formulation (solid) or fitted results from ab initio simulation (symbols) from Ref. [34]. We find that the results are in very good agreement because the total electron emission probability is mainly controlled by region I, and the profile of the static potential barrier does not have a major impact on the final results. Finally, we have only considered side-band electrons in the present work and the extension to include center band electrons will be studied in the future.

We would like to discuss the experimental realization of our model by showing that the proposed method and range of parameters are within the reach of current technology. Firstly, we note that the vertically well-aligned single-layer graphene considered in our model has been recently fabricated in arrays with H between 50 and 800 nm [33]. In our model (region I), a time-oscillating potential barrier $V = V_0 + V_1 \cos \omega t$ is taken into account, in which $V_0 = 0.2$ eV is a rectangular potential barrier and can be created by an electric field using a thin insulator or by local chemical doping [7,10,35]. A well-defined barrier can be realized by having an electric field perpendicular to the graphene sheet with an amplitude of around 5×10^{-2} V/nm, which is routinely used in experiments [7,35]. The electron concentration around the barrier is typically around 10^{12} cm^{-1} with corresponds to a Fermi energy of ≈0.083 eV in the monolayer graphene sheet. The time-oscillating barrier can be manipulated by using ultrafast lasers or other sources [36]. The very long mean free path (0.4–10 μm) in graphene makes the experimental measurement of the current predicated by our model feasible [27,28].

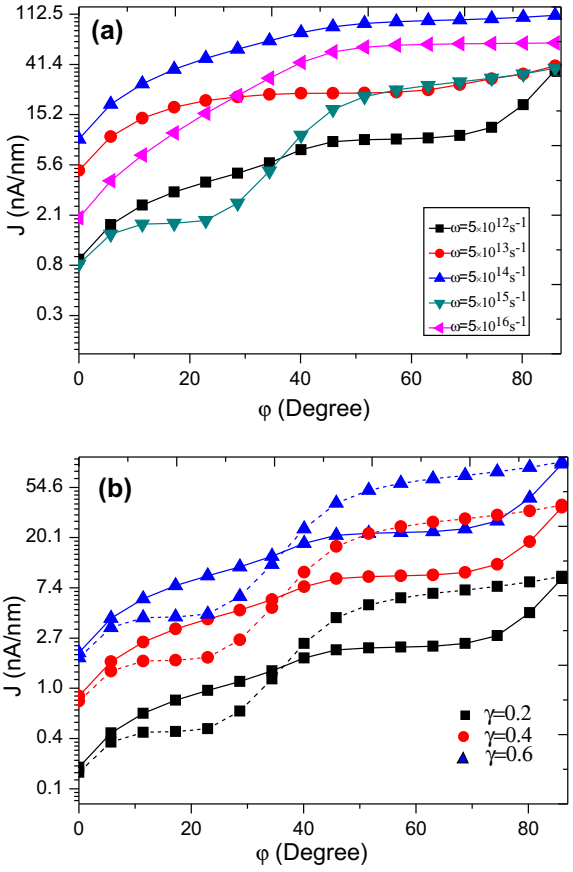

Fig. 3 – The emission current line density J [nA/nm] as a function of incident angle φ for (a) different frequency ω at $\gamma = V_1/\hbar\omega = 0.5$; and (b) different γ at ω [rad/s] = 5×10^{15} (dashed lines) and 5×10^{12} (solid lines).

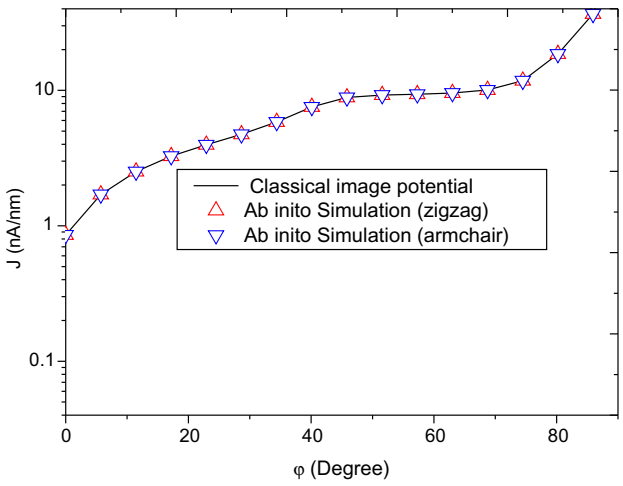

Fig. 4 – A comparison is made between our results (solid) and ab initio simulation results (symbols) from Fig. 7 in Ref. [34]. △ and ▽ is fitted to result from Fig. 7(a) and (b), respectively.

4. Conclusion

We have presented a model to describe over-barrier electron emission from the edge of monolayer graphene exposed to a time-oscillating internal barrier. It is found that the emission current line density can be tuned by both the amplitude V_1 and the frequency ω of the time-varying barrier. It is not sensitive to the applied DC field. This finding may shed new light on developing photo-excited electron sources using graphene for various applications ranging from photocathodes to even the newly proposed photon-enhanced thermionic emission for solar energy conversion [37].

Acknowledgments

This work was supported by SUTD (SRG EPD 2011 014) and SUTD-MIT IDC Grant (IDG21200106 and IDD21200103). L.K. Ang would like to acknowledge the support of USA AOARD grant (11-4069). The helpful discussion with M. Ahsan Zeb is gratefully acknowledged. Additionally, we are also grateful to Mihir Pant for his critical reading of our manuscript.

REFERENCES

[1] Zhan RZ, Chen J, Deng SZ, Xu NS. Fabrication of gated CuO nanowire field emitter arrays for application in field emission display. J Vac Sci Technol B 2010;28:558–61.
[2] Wu CX, Xu WJ, Lei X, Liu CL, Wu SL, Hu WB, et al. Characteristics of an electron source of a surface-conduction electron-emitter display. J Soc Inf Display 2008;16:625–30.
[3] Wang BP, Tong LS. A study of the optimum field emitter shape for vacuum electronics applications. Appl Surf Sci 1996;94:101–6.
[4] Bauerdick S, Burkhardt C, Kern DP, Nisch W. Addressable field emitter array: a tool for designing field emitters and a multibeam electron source. J Vac Sci Technol B 2004;22:3539–42.
[5] Park JH, Son GH, Moon JS, Han JH, Berdinsky AS, Kuvshinov DG, et al. Screen printed carbon nanotube field emitter array for lighting source application. J Vac Sci Technol B 2005;23:749–53.
[6] Sun S, Ang LK. Onset of space charge limited current for field emission from a single sharp tip. Phys Plasmas 2012;19:033107–13.
[7] Novoselov KS, Geim AK, Morozov SV, Jiang D, Zhang Y, Dubonos SV, et al. Electric field effect in atomically thin carbon films. Nature 2004;306:666–9.
[8] Garaj S, Hubbard W, Reina A, Kong J, Branton D, Golovchenko JA. Graphene as a subnanometre trans-electrode membrane. Nature 2010;467:190–3.
[9] Heersche HB, Jarillo-Herrero P, Oostinga JB, Vandersypen LMK, Morpurgo AF. Bipolar supercurrent in graphene. Nature 2007;446:56–9.
[10] Novoselov KS, Geim AK, Morozov SV, Jiang D, Katsnelson MI, Grigorieva IV, et al. Two-dimensional gas of massless Dirac fermions in graphene. Nature 2005;438:197–200.
[11] Huang PY, Ruiz-Vargas CS, van der Zande AM, Whitney WS, Levendorf MP, Kevek JW, et al. Grains and grain boundaries in single-layer graphene atomic patchwork quilts. Nature 2011;469:389–92.
[12] Dikin DA, Stankovich S, Zimney EJ, Piner RD, Dommett GHB, Evmenenko G, et al. Preparation and characterization of graphene oxide paper. Nature 2007;448:457–60.
[13] Stratakis E, Eda G, Yamaguchi H, Kymakis E, Fotakis C, Chhowalla M. Free-standing graphene on microstructured silicon vertices for enhanced field emission properties. Nanoscale 2012;4:3069–74.
[14] Pandey S, Rai P, Patole S, Gunes F, Kwon GD, Yoo JB, et al. Improved electron field emission from morphologically disordered monolayer graphene. Appl Phys Lett 2012;100:043104–7.
[15] Baby TT, Ramaprabhu S. Experimental study on the field emission properties of metal oxide nanoparticle-decorated graphene. Appl Phys Lett 2012;111:034311–5.
[16] Yamaguchi H, Murakami K, Eda G, Fujita T, Guan PF, Wang WC, et al. Field emission from atomically thin edges of reduced graphene oxide. ACS Nano 2011;5:4945–52.
[17] Santandrea S, Giubileo F, Grossi V, Santucci S, Passacantando M, Schroeder T, et al. Field emission from single and few-layer graphene flakes. Appl Phys Lett 2011;98:163109–11.
[18] Baby TT, Ramaprabhu S. Cold field emission from hydrogen exfoliated graphene composites. Appl Phys Lett 2011;98:183111–3.
[19] Chen JT, Li J, Yang J, Yan XB, Tay BK, Xue QJ. The hysteresis phenomenon of the field emission from the graphene film. Appl Phys Lett 2011;99:173104–6.
[20] Fowler RH, Nordheim L. Electron emission in intense electric fields. Proc R Soc Lond B 1928;119:173–81.
[21] Sun S, Ang LK, Shiffler D, Luginsland JW. Klein tunnelling model of low energy electron field emission from single-layer graphene sheet. Appl Phys Lett 2011;99:013112–4.
[22] Sun S, Ang LK. Shot noise of low energy electron field emission due to Klein tunneling. Phys Plasmas 2012;112:016104–6.
[23] Wang WL, Peng J, Chen GH, Deng SZ, Xu NS, Li ZB. Image potentials of single-walled carbon nanotubes in the field emission condition. J Appl Phys 2008;104:034306–8.
[24] Wang WL, Qin XZ, Xu NS, Li ZB. Field electron emission characteristic of graphene. J Appl Phys 2011;109:044304–10.
[25] Koh WS, Ang LK. Quantum model of space-charge-limited field emission in a nanogap. Nanotechnology 2008;19:235402–6.
[26] Li ZB, Xu XS, Kreuzer HJ. Coherent field emission image of graphene predicted with a microscopic theory. Phys Rev B 2012;85:115427–35.
[27] Morozov SV, Novoselov KS, Katsnelson MI, Schedin F, Elias DC, Jaszczak JA, et al. Giant intrinsic carrier mobilities in graphene and its bilayer. Phys Rev Lett 2008;100:016602–5.
[28] Purewal MS, Hong BH, Ravi A, Chandra B, Hone J, Kim P. Scaling of resistance and electron mean free path of single-walled carbon nanotubes. Phys Rev Lett 2007;98:186808–11.
[29] Zeb MA, Sabeeh K, Tahir M. Erratum: Chiral tunneling through a time-periodic potential in monolayer graphene. Phys Rev B 2009;79:089903(E).
[30] Zeb MA, Sabeeh K, Tahir M. Chiral tunneling through a time-periodic potential in monolayer graphene. Phys Rev B 2008;78:165420–6.
[31] Lazur VY, Reity OK, Rubish VV. WKB method for the Dirac equation with a scalar-vector coupling. Theor Math Phys 2005;143:559–82.
[32] Katsnelson MI, Novoselov KS, Geim AK. Chiral tunnelling and the Klein paradox in graphene. Nat Phys 2006;2:620–5.
[33] Guo F, Mukhopadhyay A, Sheldon BW, Hurt RH. Vertically aligned graphene layer arrays from chromonic liquid crystal precursors. Adv Mater 2011;23:508–13.
[34] Wang WL, Li ZB. Potential barrier of graphene edges. J Appl Phys 2011;109:114308–13.
[35] Zhang Y, Tan Y, Stormer HL, Kim P. Experimental observation of the quantum Hall effect and Berry's phase in graphene. Nature 2005;438:201–4.
[36] Liu JT, Su FH, Wang H, Deng XH. Optical field modulation on the group delay of chiral tunneling in graphene. New J Phys 2012;14:013012–8.
[37] Schwede JW, Bargatin L, Riley DC, Hardin BE, Rosenthal SJ, Su Y, et al. Photon-enhanced thermionic emission for solar concentrator systems. Nat Mater 2010;9:762–7.